Langmuir

ARTICLE

pubs.acs.org/Langmuir

Sacrificial Template-Directed Fabrication of Superparamagnetic Polymer Microcontainers for pH-Activated Controlled Release of Daunorubicin

A. Chatzipavlidis,[†,‡] P. Bilalis,[‡] E. K. Efthimiadou,[‡] N. Boukos,[‡] and G. C. Kordas*[,‡]

[†]School of Chemical Engineering, National Technical University of Athens, 9 Heroon Polytechniou st., Zografos, GR-157 80 Athens, Greece

[‡]Institute of Materials Science, NCSR "Demokritos", GR-15310 Aghia Paraskevi, Athens, Greece

Supporting Information

ABSTRACT: Magnetic pH-sensitive microcontainers were produced by a four-step process. The first step involves the synthesis of citrate-modified magnetic nanoparticles via the coprecipitation method. The second step consists of the encapsulation of magnetic nanoparticles in non-cross-linked poly(methacrylic acid) (PMAA) microspheres through distillation precipitation polymerization, resulting in a core/shell structure. The third step concerns the formation of a poly(*N*,*N*′-methylenebis(acrylamide)-*co*-mathacrylic acid) (P(MBAAm-*co*-MAA)) layer on the surface of magnetic PMAA microspheres by second distillation precipitation polymerization in order to produce a trilayer hybrid microsphere. The last step deals with the removal of PMAA layer in ethanol and formation of a stable P(MBAAm-*co*-MAA) microcontainer with magnetic nanoparticles entrapped inside the formed cavity. This process is simple and leads to the formation of superparamagnetic pH-sensitive microcontainers. The structure and properties of the magnetic microcontainers were investigated by X-ray diffraction (XRD), transmission electron microscopy (TEM), scanning electron microscopy (SEM), Fourier transform infrared spectroscopy (FT-IR), vibrating sample magnetometry (VSM), and dynamic light scattering (DLS) to determine the functionalities of the hybrid structure. The magnetic pH-sensitive microcontainers were loaded with Daunorubicin and tested with respect to release rate at different pH values in order to evaluate their functionality as controlled release system.

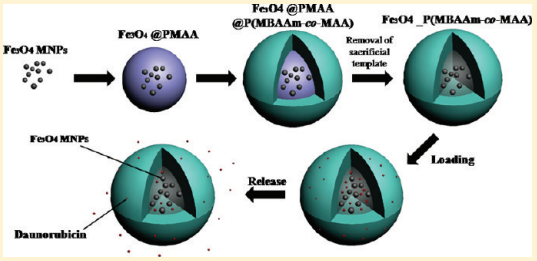

1. INTRODUCTION

Recently, significant progress has been made in the field of multi-stimuli-responsive microspheres. Because of their unique features, such as size, shape, morphology, and reliable response to various external or internal stimuli, they are utilized in a wide range of biomedical applications including drug delivery systems, biosensors, diagnostics, enzyme immobilization, etc.[1−4]

Magnetic polymer microcontainers are composed of magnetic cores entrapped in and/or on polymer shells. Each part of the system contributes its functionality to the whole structure. Specifically, the magnetic cores are composed of small clusters of magnetic nanoparticles and provide magnetic functionality to the system. In general, magnetic nanoparticles, owning to their small size, exhibit interesting physical and chemical properties, that in most cases differ dramatically from those of the corresponding bulk material.[5] Superparamagnetic behavior and quantum tunneling of magnetization are two interesting observed phenomena and can be attributed to the fact that at this size range the magnetic nanoparticles can be considered as a single magnetic domain.[6] The magnetic microcontainers can be directed to a predefined region through magnetic forces and raise the temperature of the microcontainer when exposed to alternating magnetic field.[7] The polymer shell plays the role of diamagnetic matrix in which drugs, and in general substances of biological or medical interest, can be dissolved or as a platform for binding of drugs.[8] In addition, the polymer shell provides various functionalities, such as mechanical and chemical stability, protection of the magnetic nanoparticles, and responsiveness to various stimuli such as pH or temperature changes in the environment, and offers a cavity that can be utilized as a container in order to carry drugs or other chemical substances.[9]

Various approaches have been used so far in order to fabricate magnetic polymer microspheres, including layer-by-layer deposition,[10] self-assembly of block copolymers in a selective solvent,[11] miniemulsion polymerization,[12,13] and template-assisted distillation precipitation polymerization.[14] In order to provide magnetic response to synthesized microspheres, some of the above-mentioned approaches are combined with the primary synthesis of magnetic nanoparticles and the sequential encapsulation of them inside polymer spheres.[15] In addition, research has focused on the simultaneous precipitation and encapsulation process via in situ synthesis routes. Yang et al.[16]

Received: April 5, 2011
Revised: May 20, 2011
Published: June 07, 2011

employed the chemical deposition method, which resulted in the capture of magnetic nanoparticles on the surface of the microspheres and the permeance of some others into the cavity of them. Liu et al.[17] developed an approach based on the primary encapsulation of magnetic nanoparticles inside SiO_2 microspheres produced by the Stöber method and the sequential incorporation of various (co)polymers onto the magnetic/silica seeds.

The synthetic strategy we followed for the fabrication of magnetic polymer microcontainers is the combination of synthesis, encapsulation, and selective removal of various "nanoblocks" of different sizes and shapes. Our method is based on the primary synthesis of surface-modified magnetic nanoparticles and two sequential stages of distillation precipitation polymerization in order to fabricate core/shell-type spherical structures. Further, we employed the selective dissolution of the middle layer in ethanol at room temperature, resulting in the formation of magnetic polymer hollow microspheres. Our intention was to utilize the middle layer of the final structure as a sacrificial template in order to avoid further encapsulation of the magnetic nanoparticles that may reduce the magnetic response, leading to attenuation of this important functionality. Selective dissolution of the non-cross-linked middle layer in combination with the permeability and stability of the outer cross-linked shell provided a facile method for the formation of superparamagnetic pH-sensitive microcontainers.

In the present paper, we report a facile four-step synthetic procedure for the preparation of magnetic polymer P(MBAAm-*co*-MAA) microcontainers that have both magnetic response and pH sensitivity and can be further used as containers and drug carriers. The properties of the synthesized microspheres are investigated and analyzed in order to confirm their multifunctionality. The utilization of the synthesized magnetic hollow microspheres as drug carriers was investigated by Daunorubicin loading and release. Daunorubicin (DNR) is a broadly used anticancer, antineoplastic or cytotoxic, chemotherapy drug, which is classified as an anthracycline antitumor antibiotic.[18−20] DNR is used as medication in many types of cancer and is usually employed in the synthetic procedure of other agents, such as Doxorubicin. For the above reasons, we studied DNR kinetics of loading and release in order to derive information for this family of chemorapeutic agents and their encapsulation in microcontainers.

2. EXPERIMENTAL SECTION

2.1. Materials. Ferric chloride ($FeCl_3 \cdot 6H_2O$) and ferrous chloride ($FeCl_2 \cdot 4H_2O$) were purchased from Fluka. Ammonia (25%, aqueous solution) was obtained from Panreac. 2,2′-Azobis(isobutyronitrile) (AIBN, 98%) was purchased from Acros and recrystallized from hexane and methanol. *N*,*N*′-Methylenebis(acrylamide) (MBAAm, 96%) was bought from Acros and used as received. Methacrylic acid (MAA, 99%) was obtained from Acros and purified by vacuum distillation. Trisodium citrate was obtained from Fisher Scientific and used as received. Acetonitrile (Aldich) was dried over calcium hydride and purified by distillation before use. Daunorubicin hydrochloride (DNR) was provided by Pharmacia & Upjohn and used as received.

2.2. Synthesis. *2.2.1. Synthesis of Citrate-Modified Magnetite Nanoparticles.* Citrate-modified magnetite nanoparticles, designated as Fe_3O_4 MNPs, were prepared by chemical coprecipitation of Fe^{3+} and Fe^{2+} ions under basic conditions.[21] Briefly, $FeCl_3 \cdot 6H_2O$ (12.0 g, 44 mmol) and $FeCl_2 \cdot 4H_2O$ (4.90 g, 24 mmol) were dissolved in 50 mL of deionized water under ultrasonication with mechanical stirring at 80 °C, and then 63 mL of ammonia (25 wt %) aqueous solution was added. The dispersion was stirred for 30 min upon addition of trisodium citrate (1.40 g, 5 mmol). The precipitated nanoparticles were washed several times with deionized water and separated by magnetic decantation. Finally, magnetic nanoparticles were dried under vacuum at 60 °C.

2.2.2. Synthesis of Monodisperse Fe_3O_4@PMAA Core/Shell Microspheres by Distillation Precipitation Polymerization. Magnetic polymer core/shell microspheres, designated as Fe_3O_4@PMAA core/shell microspheres, were prepared by distillation precipitation polymerization in acetonitrile with AIBN as initiator in the presence of citrate-modified Fe_3O_4. The polymerization procedure was accomplished as follows: MAA (2 mL, 23 mmol) and trisodium citrate-modified Fe_3O_4 (0.01 g) were dispersed in 80 mL of acetonitrile at room temperature in a 250 mL two-necked flask. After the homogenization of the suspension by ultrasonic treatment for 10 min, AIBN (0.05 g, 0.3 mmol, 2.5 wt % relative to the monomer) was added, and the flask was equipped with a fractionating column, Liebig condenser, and a receiver. Mechanical stirring was employed during the preparation procedure. The flask was submerged in a heating mantle, and the polymerization mixture was heated from ambient temperature until boiling state within 30 min. The polymerization was continued further under boiling state for 20 min when the solvent was distilled from the reaction system. The reaction was ended after 40 mL of acetonitrile was distilled off the reaction mixture within 1 h. After the reaction, the resultant Fe_3O_4@PMAA core−shell hybrid microspheres were purified by five cycles of ultracentrifugation, decanting, and redispersion in acetonitrile with ultrasonic bathing.

2.2.3. Synthesis of Fe_3O_4@PMAA@P(MBAAm-co-MAA) Trilayer Microspheres by the Second-Stage Distillation Precipitation Polymerization. A typical procedure for the distillation precipitation polymerization to afford Fe_3O_4@PMAA@P(MBAAm-*co*-MAA) trilayer microspheres was accomplished as follows: 0.13 g of Fe_3O_4@PMAA microspheres was suspended in 70 mL of acetonitrile as a brown suspension for the seeds of the second-stage polymerization. Then, MAA (0.30 mL, 3.5 mmol), MBAAm (0.07 g, 0.4 mmol), and AIBN (0.01 g, 0.06 mmol, and 2.7 wt % relative to the monomers) were dissolved in the suspension. The same procedure as previously described was followed. The polymerization was carried out with distilling the solvent out of the reaction system, and the reaction was ended after 35 mL of acetonitrile was distilled off the reaction mixture within 1 h. After the polymerization, the resultant Fe_3O_4@PMAA@P(MBAAm-*co*-MAA) trilayer microspheres were separated and purified by repeating centrifugation, decanting, and resuspension in acetonitrile with ultrasonic bathing for three times. The trilayer particles were dried in vacuum at room temperature until constant weight.

2.2.4. Preparation of Fe_3O_4_P(MBAAm-co-MAA) Microcontainers. The resultant Fe_3O_4@PMAA@P(MBAAm-*co*-MAA) trilayer microspheres were dialyzed in ethanol at room temperature for selective dissolution of PMAA middle layer. The dialysis process to obtain Fe_3O_4_P(MBAAm-*co*-PMAA) microcontainers lasted 3 days for complete removal of PMAA middle layer. The resulting product was dried in vacuum at room temperature until constant weight.

2.2.5. Preparation of DNR-Loaded Fe_3O_4_P(MBAAm-co-MAA) Microcontainers. DNR-loaded Fe_3O_4_P(MBAAm-*co*-MAA) microcontainers were prepared by a previously described method.[22] Briefly, daunorubicin hydrochloride (DNR, 0.20 mg) was dissolved in 10 mL of a NaCl solution 0.9 wt %, and then 8.0 mg of Fe_3O_4_P(MBAAm-*co*-MAA) microcontainers was suspended in this solution. The loading of the drug took place in the suspension on a shaker with gentle agitation for 3 days. The percentage of DNR on P(MBAAm-*co*-MAA) microcontainers was determined by a UV−vis spectrometer. The unloaded DNR was removed by centrifugation. The loading capacity was calculated by the difference of DNR concentration between the standard DNR solution and the supernatant after loading.

Scheme 1. Schematic Illustration of (a) the Four-Step Procedure for the Fabrication of Fe_3O_4_P(MBAAm-*co*-MAA) Microcontainers and (b) the Chemical Structure of Daunorubicin (DNR)

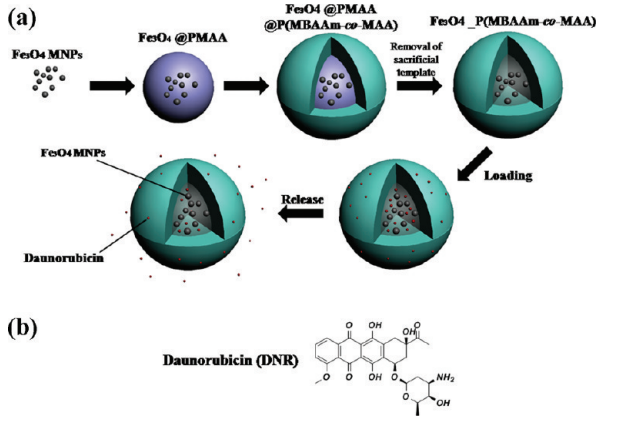

2.2.6. In vitro Release of DNR. DNR release tests were carried out as follows: in 10 mL of phosphate-buffered solution, pH = 7.4, 5 mg of DNR-loaded microcontainers was dispersed, and a portion of the solution was removed periodically from the solution and was centrifuged. The release of DNR from the microcontainers was calculated by ultraviolet spectroscopy measurements of the supernatant solution. The same procedure was followed for the release study in an acidic buffer, pH = 4.5.

2.3. Characterizations. X-ray diffraction (XRD) measurements were made using a Siemens D-500 diffractometer using Cu Kα radiation (λ = 1.5418 Å). Transmission electron microscopy (TEM) was used in order to specify size and morphology of the synthesized microcontainers. TEM samples were prepared by placing one drop of diluted sample on a carbon-coated grid and leaving the solvent to evaporate. Scanning electron microscopy (SEM) images were obtained with a view to maintain complementary data on the size and morphology studies. We used a Phillips Quanta Inspect (FEI Company) microscope with W (tungsten) filament 25 kV. Fourier transform infrared spectra (FT-IR) were collected over the range of 4000−380 cm^{-1} using a Perkin-Elmer Precisely Spectrum 100 spectrometer. The magnetic properties of the nanostructures were studied using vibrating sample magnetometry (VSM) at room temperature. A VSM model 155 with a Bell 640 Gmeter, source Danfysik System 8000 (−2 to 2 T) (A/S, Mollehaven 31, DK-4040 Jyllinge, Denmark) was equipped in order to record the magnetic loops. Dynamic light scattering (DLS) measurements were performed by a Zetasizer Nano from Malvern Instruments in order to study the response of P(MBAAm-*co*-MAA) microcontainers in different pH environments and to measure the hydrodynamic diameter (D_h) and the polydispersity index of the size distribution. UV−vis absorption spectra were measured on a Thermo UV−vis spectrometer at 233 nm for the determination of DNR. For the synthetic procedure, we used deionized water (Millipore, Milli-Q), and the homogenization of the suspensions, when needed, took place in an ultrasonic processor (Elma Sonic Bath, S.30H).

3. RESULTS AND DISCUSSION

Scheme 1 illustrates the synthesis procedure of the Fe_3O_4_P(MBAAm-*co*-MAA) microcontainers and the chemical structure of Daunorubicin. The procedure consists of four steps: (1) preparation of citrate-modified magnetite nanoparticles via chemical coprecipitation of Fe^{3+} and Fe^{2+} ions under basic conditions, (2) encapsulation of magnetic nanoparticles into non-cross-linked PMAA microspheres by first-stage distillation precipitation polymerization, resulting in core/shell structure, (3) formation of Fe_3O_4@PMAA@P(MBAAm-*co*-MAA) trilayer microspheres by the second-stage distillation precipitation polymerization, and (4) selective removal of the noncross-linked PMAA core, resulting in the formation of P(MBAAm-*co*-MAA) microcontainers with magnetic nanoparticles entrapped within the configured cavity.

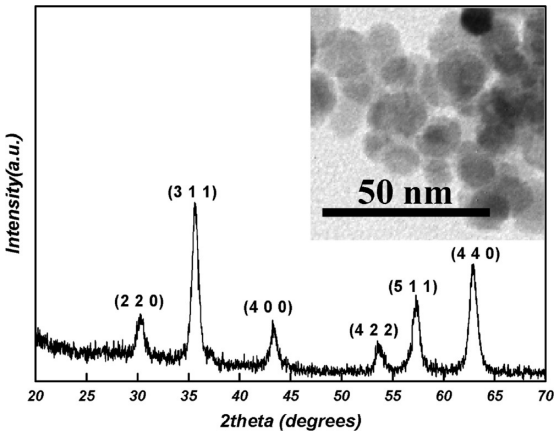

Figure 1. XRD pattern of the Fe_3O_4 MNPs. Inset shows TEM micrograph of nanoparticles under study.

Figure 1 shows the XRD pattern and TEM micrograph of the iron oxide nanoparticles used as seeds during the first-stage distillation precipitation polymerization. The observed peaks are the same as those reported for standard bulk Fe_3O_4 (JCPDS, card 79-0419). The sharpness and the intensity of the diffraction peaks confirm the good crystallinity of the synthesized magnetic nanoparticles. The broadening of the peaks is mainly attributed to the small size of the crystallite. The application of the Scherrer formula to the most intense line (311) of the spinel structure yields for D the value of 12 nm. This value agrees well with the TEM measurements of the synthesized nanoparticles (Figure 1, inset).

The fabricated Fe_3O_4@PMAA microspheres exhibit a core/shell type structure with arranged spherical shape and smooth morphology. Figure 2a,b shows the SEM and TEM micrographs of the well-shaped core/shell microspheres exhibiting an average size of 260 nm. The dark region in the center corresponds to the aggregates formed by magnetic nanoparticles. Different contrast between the core and shell is attributed to different electron penetration efficiency of magnetite nanoparticles and PMAA shell. The magnetic nanoparticles exhibit formation of chainlike structures and clustering due to magnetic interactions.[23]

Concerning the magnetic content, various control experiments were made in order to optimize the fabricated microspheres. Specifically, the modulation of the magnetic content of the microspheres was studied during the second step of the synthetic procedure by changing the amount of citrate-stabilized MNPs used as seeds. SEM images revealed that in the first case (0.01 g of citrate-stabilized MNPs) no magnetic nanoparticles or aggregates of them were observed near or on the surface of the microspheres (Figure 2a). In two other cases, where 0.03 and 0.05 g of citrate-stabilized MNPs were used as seeds, the formation of aggregates in the proximity or on the surface of

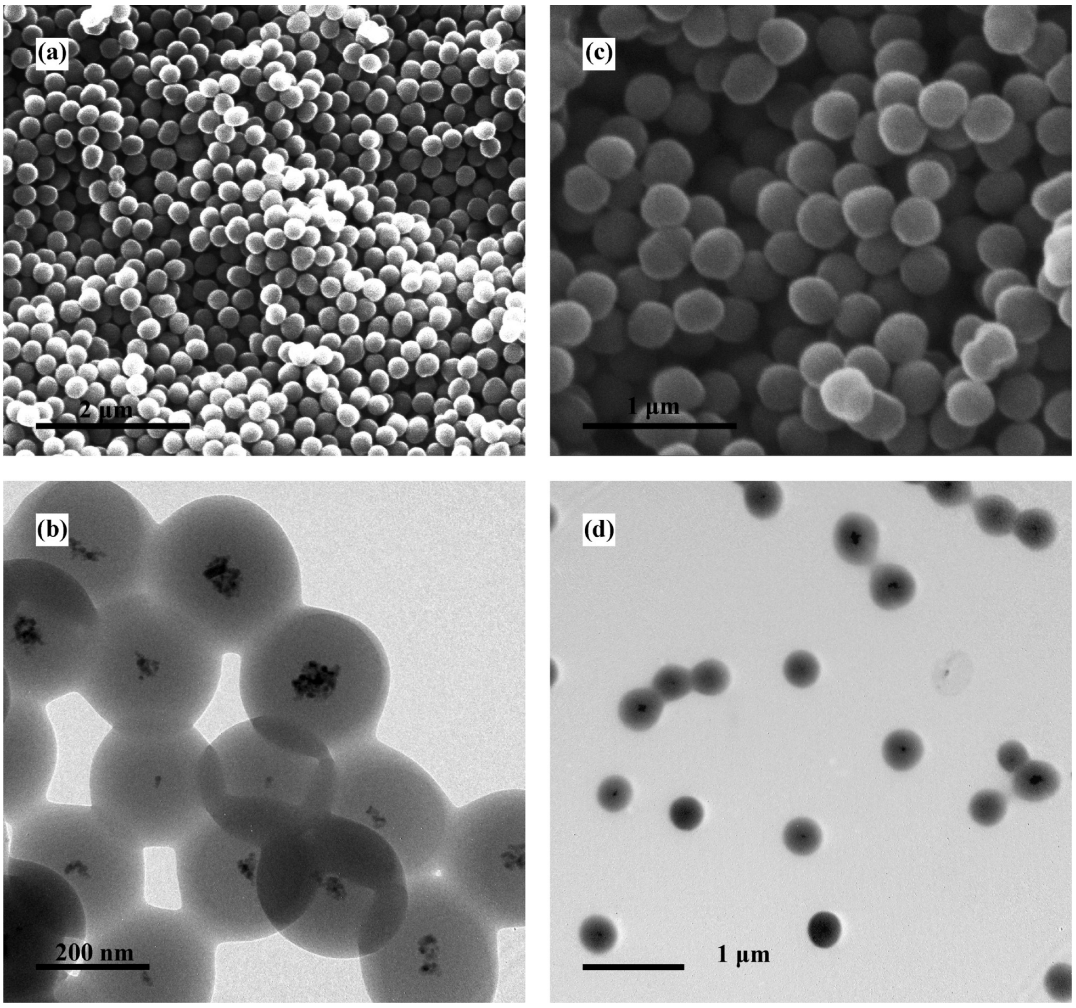

Figure 2. (a) SEM and (b) TEM micrograph of Fe_3O_4@PMAA core/shell microspheres. (c) SEM and (d) TEM micrograph of Fe_3O_4@PMAA@P(MBAAm-*co*-MAA) trilayer microspheres.

Fe_3O_4@PMAA microspheres (Supporting Information Figures 2a and 2b, respectively) was observed.

The confinement of magnetic aggregates' size was achieved through the surface modification of magnetic nanoparticles with trisodium citrate. The selection of trisodium citrate was based on its carboxyl groups that provide functional groups and negative charge on the surface, leading to a better dispersion.[24,25] In this way, the synthesized magnetic nanoparticles formed sufficiently smaller aggregates, and the modulation of magnetic content of the microcontainers is more controllable. Moreover, the presence of citrate molecules is important for the subsequent coating with polymer shell and the formation of core/shell-type structure.[26] As reported in other studies,[27] it is very important to control the formation of clusters of magnetic nanoparticles entrapped in other nanostructures. In order to obtain superparamagnetic Fe_3O_4 nanoparticles and maintain the superparamagnetic behavior in the sequential structures, their size should be below a critical value, around 12 nm.[29] The size of the aggregates should be large enough in order to show essential magnetic response for application such as separation and guidance by external magnetic field. Further, aggregates should be small enough in order maintain the small size range of the resulting composite nanostructure and to provide efficient response in the aforementioned processes. DLS measurements were conducted in order to examine the influence of citrate stabilization on the dispersity of magnetic nanoparticles and the possible formation of aggregations (see Supporting Information Figure 1). The existence of two average diameters (11.8 and 78.8 nm) is attributed to the formation of small aggregates due to short-range attractive van der Waals forces.[28]

Figures 2c and 2d illustrate the formation of a thin P(MBAAm-*co*-MAA) shell layer around the previously described core/shell nanostructure showing that the trilayer structure was successfully fabricated. The increase of the mean diameter of the core/shell particle, measured by SEM micrograph analysis, in combination with the corresponding TEM micrograph, confirms the above assumption. Specifically, the average size is ~300 nm. The smoothness of the morphology is attributed to the template-assisted polymerization on the well-shaped Fe_3O_4@PMAA templates.

The final stage of the synthetic procedure includes the selective removal of non-cross-linked PMAA core and the formation of P(MBAAm-*co*-MAA) shell containing magnetic nanoparticles in the formed cavity. Figure 3 shows the TEM micrograph of the Fe_3O_4_P(MBAAm-*co*-MAA) microcontainers indicating that the non-cross-linked PMAA sacrificial template

dx.doi.org/10.1021/la201240h |*Langmuir* 2011, 27, 8478–8485

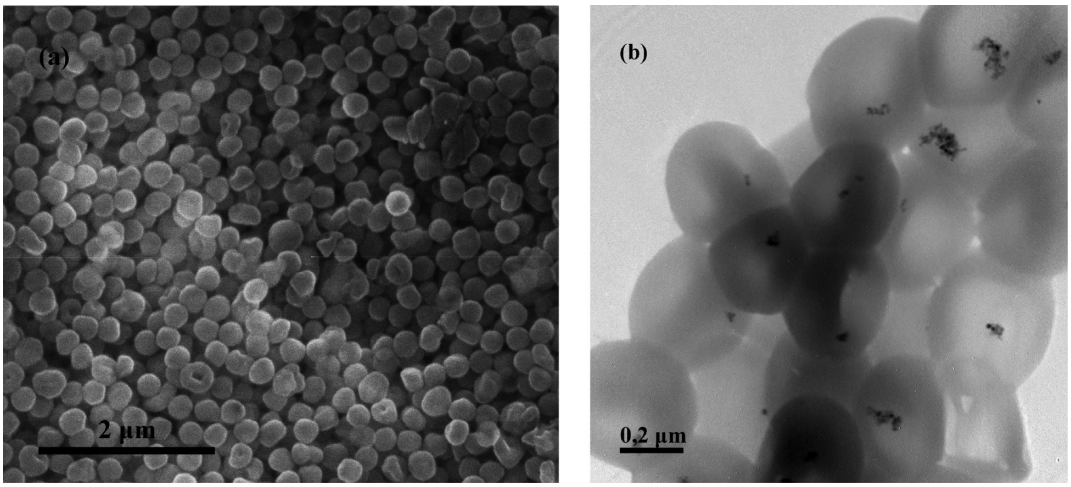

Figure 3. (a) SEM and (b) TEM micrographs of Fe_3O_4_P(MBAAm-*co*-MAA) microcontainers.

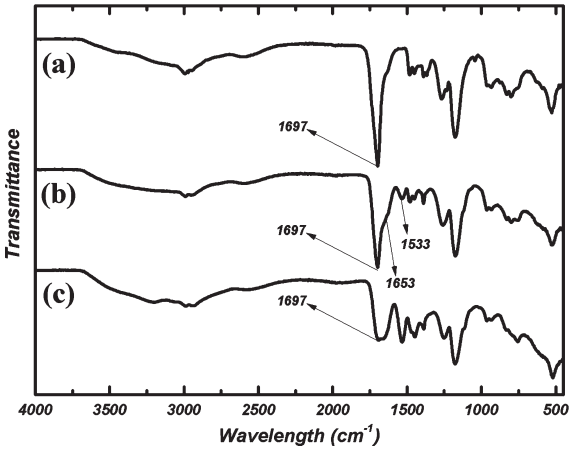

Figure 4. FT-IR spectra of (a) Fe_3O_4@PMAA core/shell microspheres, (b) Fe_3O_4@PMAA@P(MBAAm-*co*-MAA) trilayer microspheres, and (c) Fe_3O_4_P(MBAAm-*co*-MAA) microcontainers.

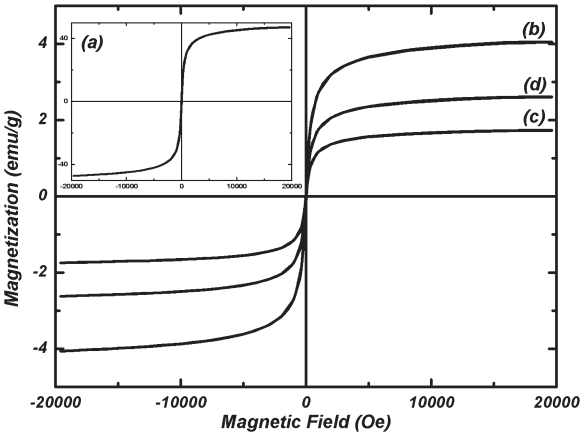

Figure 5. Magnetization curves of (a) Fe_3O_4 MNPs, (b) Fe_3O_4@PMAA core/shell microspheres, (c) Fe_3O_4@PMAA@P(MBAAm-*co*-MAA) trilayer microspheres, and (d) Fe_3O_4_P(MBAAm-*co*-MAA) microcontainers.

was effectively removed and left behind sufficient amount of Fe_3O_4 MNPs. The P(MBAAm-*co*-MAA) shell resisted the collapse and maintained spherical shape. The thickness of the shell is ~40 nm, and this was estimated by the comparison of SEM images before and after the selective removal of the sacrificial template. One can perceive from this figure a good distribution of the magnetic content in the sample. This is crucial to ensure magnetic response for all synthesized microcontainers. The slight deformation of the microcontainers is attributed to measurement conditions during TEM analysis that deform the relative thin shells of the microcontainers.

FT-IR spectroscopy confirmed the successful fabrication of the microcontainers. Figure 4 shows the FT-IR spectra of the seeded copolymerization of MBAAm and MAA leading to Fe_3O_4@PMAA@P(MBAAm-*co*-MAA) trilayer microspheres. The peak at 1697 cm^{-1} (Figure 4a) corresponds to the characteristic stretching vibration of the carbonyl group of the middle layer PMAA segments. Figure 4b shows two additional peaks at 1533 and 1653 cm^{-1} due to the vibration of the amide group of PMBAAm segments. This result proves the formation of the shell layer during the second-stage distillation precipitation polymerization. The considerable decrease of the peak at 1697 cm^{-1} in Figure 4c is due the successful removal of the PMAA middle layer by dissolution in ethanol, leading to the formation of the resultant hybrid magnetic microcontainers.

Figure 5 shows the room temperature magnetic field vs magnetization curves for the products of each step of the synthesis procedure. All four curves have an S-shape at low-field region and are almost linear in the high-field region. Furthermore, all samples show negligible values of remnant magnetization and coercivity. The above characteristics of the curves indicate the superparamagnetic behavior of the synthesized composite microspheres.[30] The measured saturation magnetization of Fe_3O_4 MNPs is 47.1 emu/g. This reduction compared to bulk value of saturation magnetization (~90 emu/g)[31] is attributed to surface effects such as surface spin canting, surface disorder, adsorbed molecules, cation size distribution, and stoichiometry deviation that affect the magnetic properties of MNPs.[32] The saturation magnetization of Fe_3O_4_P(MBAAm-*co*-MAA) microcontainers is higher than that of the Fe_3O_4@PMAA@P(MBAAm-*co*-MAA) trilayer microspheres, and this supports our assumptions that the PMAA second layer was successfully removed, leaving behind sufficient magnetic content.

dx.doi.org/10.1021/la201240h |*Langmuir* 2011, 27, 8478–8485

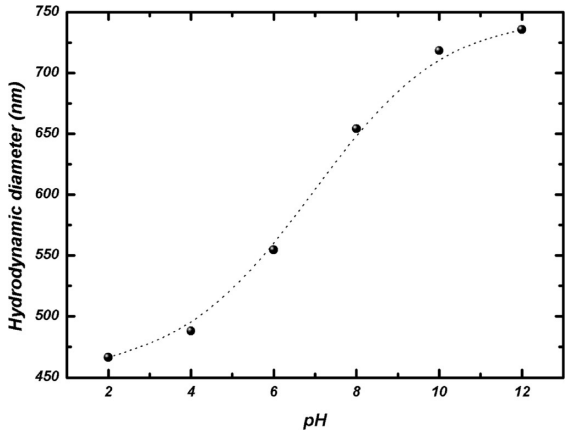

Figure 6. pH dependence of the hydrodynamic diameter of Fe_3O_4_P(MBAAm-*co*-MAA) microcontainers measured at 25 °C.

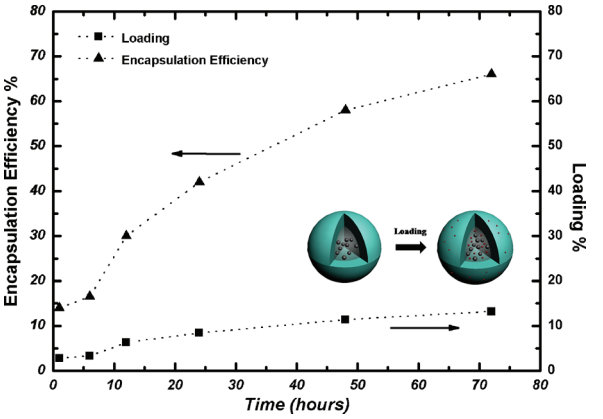

Figure 7. Loading capacity and encapsulation efficiency of DNR of Fe_3O_4_P(MBAAm-*co*-MAA) microcontainers in different correlation times. Inset is the schematic model of loading procedure.

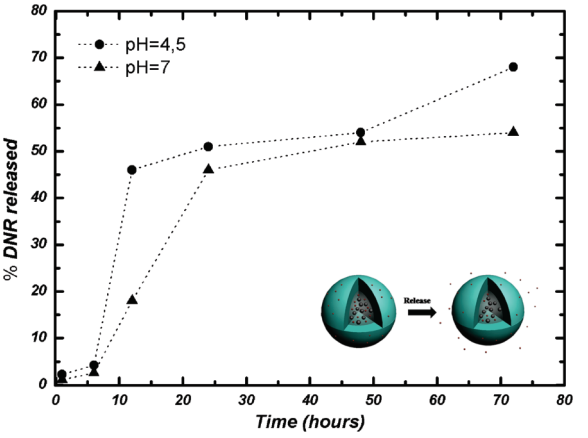

Figure 8. Controlled release of DNR from Fe_3O_4_P(MBAAm-*co*-MAA) microcontainers under different pH conditions. Inset is the schematic model of release procedure.

The utilization of Fe_3O_4@PMAA microspheres as templates for the second stage distillation precipitation polymerization in combination with the selective removal of the middle non-cross-linked layer resulted in the conservation of the superparamagnetic behavior and avoidance of undesirable attenuation of the magnetic response. For the sake of comparison, studies by other groups on hybrid magnetic micro- or nanospheres are reported.[14,16,33−35] Further studies on magnetic properties of the nanoparticles, used as seeds during the first distillation precipitation polymerization, might be a way to optimize the magnetic response of the synthesized structures.

One of the basic requirements for the use of the fabricated microcontainers as drug carriers and controlled release systems is their sensitivity toward changes of the pH values of their environment. Figure 6 shows DLS measurements of the size of the Fe_3O_4_P(MBAAm-*co*-MAA) microcontainers as a function of the pH. The data points of this figure present average values of 10−20 measurements with a 20 s integration. All DLS measurements exhibit a narrow size distribution with polydispersity index less than 0.09. The hydrodynamic diameter of Fe_3O_4_P(MBAAm-*co*-MAA) microcontainers increased from 466.5 nm at pH of 2 to 554.7 nm at pH of 6 to 735.8 nm at pH of 12. The measured changes of diameters under different pH values are attributed to the Donnan osmotic swelling of the polymer network of the P(MBAAm-*co*-MAA) shell, which is ascribed to the partial ionization of the PMAA segments that are present in the P(MBAAm-*co*-MAA) shell.[36,37] The difference between hydrodynamic diameters measured by DLS and diameters calculated by TEM and SEM micrographs is mainly related to the swollen state of microcontainers dispersed in aqueous solutions during DLS measurements. The reported pH-sensitive behavior can be validated as an important functionality of the microcontainers and can be utilized in order to use them as drug carriers.

In order to evaluate the application of Fe_3O_4_P(MBAAm-*co*-MAA) microcontainers as drug carriers, we performed loading and release study, using DNR as cargo (Figure 1b). Figure 7 shows the loading capacity of the DNR on microcontainers via spectrometric analysis as a function of the time. One can perceive from this figure a steady increase of load from 2.8% at 1 h to 13.2% at 72 h. In addition, the encapsulation efficiency reached 66% at 72 h.

Figure 8 shows the drug release rate of DNR from the Fe_3O_4_P (MBAAm-*co*-MAA) microcontainers at pH 4.5 and 7. We chose these pH values in order to simulate the slightly acidic environment of tumors.[38] DNR released very slowly from microcontainers, and the release rate leveled off after 2 h under neutral condition (pH = 7.4, phosphate buffer). The starting point of the release is at the first 30 min. However, the release percentage was too low for monitoring. First only 18% of the loaded DNR was released from microcontainers even after 12 h. After 24, 48, and 72 h, 46%, 52%, and 54% was released from the microcontainers, respectively. Figure 8 also suggests that in the acidic conditions the drug was released faster than in the case of neutral conditions. More precisely, after 2 h the drug released to an amount of 46%. A release of 51%, 54%, and 68% of the total loaded DNR drug was observed at 24, 48, and 72 h, respectively. The kinetics study of the DNR release indicates a pH dependence of release process. This result confirms the assumption that the pH sensitivity of the synthesized microcontainer can be a tunable property triggering controlled release.

The surface chemistry of Fe_3O_4_P(MBAAm-*co*-MAA) microcontainers suggests that hydrogen-bonding interaction takes place between the functional groups on the surface of the shell and DNR molecules. Specifically, the loading of DNR on the surface of Fe_3O_4_P(MBAAm-*co*-MAA) microspheres is assigned to hydrogen-bonding interaction between carboxyl and amide

groups of the shell and both hydroxyl and amino groups of DNR molecules. As reported in previous studies,[14,23] the contribution of each hydrogen-bonding interaction depends on protonization and ionization processes that may take place in acidic, neutral, or basic conditions. Further, the considerable dependence of the release behavior of DNR drug from Fe_3O_4_P(MBAAm-*co*-MAA) microcontainers on pH values of their environment may originate from the difference of the strength for the hydrogen-bonding interaction between the carboxyl groups of the microcontainers and functional groups (amine, hydroxyl) of DNR molecules, under different pH conditions. The reported results demonstrated that the basic mechanism that designated the controlled release is the pH sensitivity of the microcontainers and the binding of the drug, rather than other physical or chemical mechanisms, such as diffusion or degradation of the polymer shell.

4. CONCLUSIONS

We have successfully fabricated, via a sacrificial template-directed procedure, magnetic microcontainers and evaluated their multifunctionality with various characterization techniques. The microcontainers exhibited good distribution of magnetic content, superparamagnetic characteristics, and pH-sensitive behavior. DNR loading and release studies have shown that pH sensitivity of the microcontainers could be utilized as a controlled release mechanism.

■ ASSOCIATED CONTENT

Supporting Information. Intensity size distribution of citrate-stabilized magnetic nanoparticles versus particle diameter and SEM images of Fe_3O_4@PMAA core/shell microspheres using different amounts of citrate-stabilized magnetic nanoparticles as seeds. This material is available free of charge via the Internet at http://pubs.acs.org.

■ AUTHOR INFORMATION

Corresponding Author

*Tel: +30210 6503336; Fax: +30210 6547690; e-mail: gkordas@ims.demokritos.gr.

■ ACKNOWLEDGMENT

We thank the European Research Council (ERC) for financial support of this work under the "IDEAS" project called "A Novel Nano-container drug carrier for targeted treatment of prostate cancer" with the acronym NANOTHERAPY and the reference number 232959.

■ REFERENCES

(1) Gil, P. R.; del Mercato, L. L.; del Pino, P.; Muñoz Javier, A.; Parak, W. J. *Nano Today* **2008**, *3*, 12–21.

(2) Liu, T.-Y.; Hu, S.-H.; Liu, D.-M.; Chen, S.-Y.; Chen, I.-W. *Nano Today* **2009**, *4*, 52–65.

(3) Sukhorukov, G.; Rogach, A.; Garstka, M.; Springer, S.; Parak, W.; Muñoz-Javier, A.; Kreft, O.; Skirtach, A.; Susha, A.; Ramaye, Y.; Palankar, R.; Winterhalter, M. *Small* **2007**, *3*, 944–955.

(4) (a) Sukhorukov, G.; Rogach, A.; Zebli, B.; Liedl, T.; Skirtach, A.; Köhler, K.; Antipov, A.; Gaponik, N.; Susha, A.; Winterhalter, M.; Parak, W. *Small* **2005**, *1*, 194–200. (b) Gorin, D. A.; Portnov, S. A.; Inozemtseva, O. A.; Luklinska, Z.; Yashchenok, A. M.; Pavlov, A. M.; Skirtach, A. G.; Mohwald, H.; Sukhorukov, G. B. *Phys. Chem. Chem. Phys.* **2008**, *10*, 6899–6905. (c) Skirtach, A. G.; Muñoz Javier, A.; Kreft, O.; Köhler, K.; Piera Alberola, A.; Möhwald, H.; Parak, W. J.; Sukhorukov, G. B. *Angew. Chem., Int. Ed.* **2006**, *45*, 4612–4617.

(5) (a) O'Handley, R. C. *Modern Magnetic Materials: Principles and Applications*; Wiley: New York, 2000. (b) Gubin, S. P.; Koksharov, Y. A.; Khomutov, G. B.; Yurkov, G. Y. *Russ. Chem. Rev.* **2005**, *74*, 489–520.

(6) (a) Kodama, R. H. *J. Magn. Magn. Mater.* **1999**, *200*, 359–372. (b) Lu, A.-H.; Salabas, E.; Schüth, F. *Angew. Chem., Int. Ed.* **2007**, *46*, 1222–1244.

(7) Laurent, S.; Forge, D.; Port, M.; Roch, A.; Robic, C.; Vander Elst, L.; Muller, R. N. *Chem. Rev.* **2008**, *108*, 2064–2110.

(8) Duncan, R. *Nat. Rev. Drug Discovery* **2003**, *5*, 347–360.

(9) (a) You, J.-O.; Almeda, D.; Ye, G. J. C.; Auguste, D. T. *J. Biol. Eng.* **2010**, *4*, 15–26. (b) Bedard, M. F.; Munoz-Javier, A.; Mueller, R.; del Pino, P.; Fery, A.; Parak, W. J.; Skirtach, A. G.; Sukhorukov, G. B. *Soft Matter* **2009**, *5*, 148–155. (c) Fu, G.-D.; Li, G. L.; Neoh, K. G.; Kang, E. T. *Prog. Polym. Sci.* **2011**, *36*, 127–167.

(10) (a) Tang, Z.; Wang, Y.; Podsiadlo, P.; Kotov, N. A. *Adv. Mater.* **2006**, *18*, 3203–3224. (b) Abbasi, A. Z.; Gutiérrez, L.; del Mercato, L. L.; Herranz, F.; Chubykalo-Fesenko, O.; Veintemillas-Verdaguer, S.; Parak, W. J.; Morales, M. P.; González, J. M.; Hernando, A.; de la Presa, P. *J. Phys. Chem. C* **2011**, *115* (14), 6257–6264.

(11) Liu, T.-Y.; Liu, K.-H.; Liu, D.-M.; Chen, S.-Y.; Chen, I.-W. *Adv. Funct. Mater.* **2009**, *19*, 616–623.

(12) Zheng, W.; Gao, F.; Gu, H. *J. Magn. Magn. Mater.* **2005**, *288*, 403–410.

(13) Sun, Y.; Wang, B.; Wang, H.; Jiang, J. *J. Colloid Interface Sci.* **2007**, *308*, 332–336.

(14) Yang, X.; Chen, L.; Huang, B.; Bai, F.; Yang, X. *Polymer* **2009**, *50*, 3556–3563.

(15) Liu, G.; Wang, H.; Yang, X. *Polymer* **2009**, *50*, 2578–2586.

(16) Yang, X.; Chen, L.; Han, B.; Yang, X.; Duan, H. *Polymer* **2010**, *51*, 2533–2539.

(17) Liu, G.; Wang, H.; Yang, X.; Li, L. *Eur. Polym. J.* **2009**, *45*, 2023–2032.

(18) Minotti, G.; Menna, P.; Salvatorelli, E.; Cairo, G.; Gianni, L. *Pharmacol. Rev.* **2004**, *56*, 185–229.

(19) Aubel-Sadron, G.; Londos-Gagliardi, D. *Biochimie* **1984**, *66*, 333–352.

(20) Monneret, C. *Eur. J. Med. Chem.* **2001**, *36*, 483–493.

(21) Sauzedde, F.; Elaïssari, A.; Pichot, C. *Colloid Polym. Sci.* **1999**, *277*, 846–855.

(22) Li, G.; Yang, X.; Wang, B.; Wang, J.; Yang, X. *Polymer* **2008**, *49*, 3436–3443.

(23) Schmidt, A. M. *Colloid Polym. Sci.* **2006**, *285*, 953–966.

(24) Yang, L.; Guo, C.; Jia, L.; Xie, K.; Shou, Q.; Liu, H. *Ind. Eng. Chem. Res.* **2010**, *49*, 8518–8525.

(25) Dubois, E.; Cabuil, V.; Boué, F.; Perzynski, R. *J. Chem. Phys.* **1999**, *111*, 7147–7160.

(26) Hong, R.-Y.; Li, J.-H.; Zhang, S.-Z.; Li, H.-Z.; Zheng, Y.; Ding, J.-M.; Wei, D.-G. *Appl. Surf. Sci.* **2009**, *255*, 3485–3492.

(27) Ditsch, A.; Laibinis, P. E.; Wang, D. I. C.; Hatton, T. A. *Langmuir* **2005**, *21*, 6006–6018.

(28) Tural, B.; Özkan, N.; Volkan, M. *J. Phys. Chem. Solids* **2009**, *70*, 860–866.

(29) Bédard, M. F.; Braun, D.; Sukhorukov, G. B.; Skirtach, A. G. *ACS Nano* **2008**, *2*, 1807–1816.

(30) Goya, G. F.; Grazú, V.; Ibarra, M. R. *Curr. Nanosci.* **2008**, *4*, 1–16.

(31) Simeonidis, K.; Mourdikoudis, S.; Moulla, M.; Tsiaoussis, I.; Martinez-Boubeta, C.; Angelakeris, M.; Dendrinou-Samara, C.; Kalogirou, O. *J. Magn. Magn. Mater.* **2007**, *316*, e1–e4.

(32) Morales, M. P.; Veintemillas-Verdaguer, S.; Montero, M. I.; Serna, C. J.; Serna, C. J.; Roig, A.; Casas, Ll.; Martínez, B.; Sandiumenge, F. *Chem. Mater.* **1999**, *11*, 3058–3064.

(33) Lien, Y.-H.; Wu, T.-M. *J. Colloid Interface Sci.* **2008**, *326*, 517–521.

(34) Mu, B.; Liu, P.; Dong, Y.; Lu, C.; Wu, X. *J. Polym. Sci., Polym. Chem.* **2010**, *48*, 3135–3144.
(35) Liu, B.; Yang, X.; Ji, H. *Polym. Int.* **2010**, *59*, 961–966.
(36) Sauer, M.; Streich, D.; Meier, W. *Adv. Mater.* **2001**, *13*, 1649–1651.
(37) Schmaljohann, D. *Adv. Drug Delivery Rev.* **2006**, *58*, 1655–1670.
(38) Zheng, C.; Xu, J.; Yao, X.; Xu, J.; Qiu, L. *J. Colloid Interface Sci.* **2011**, *355*, 374–382.